ELSEVIER

Journal of Nuclear Materials 277 (2000) 263–273

journal of nuclear materials

www.elsevier.nl/locate/jnucmat

Estimation of fracture toughness transition curves of RPV steels from ball indentation and tensile test data

Thak Sang Byun[a,*], Seok Hun Kim[b], Bong Sang Lee[a], In Sup Kim[b], Jun Hwa Hong[a]

[a] *Reactor Materials Department, Korea Atomic Energy Research Institute, P.O. Box 105, Yusong, Taejon 305-600, South Korea*
[b] *Department of Nuclear Engineering, Korea Advanced Institute of Science and Technology, 373-1 Kusong-dong, Yusong-gu, Taejon, South Korea*

Received 15 February 1999; accepted 13 July 1999

Abstract

It was attempted to estimate the fracture toughness transition curves of reactor pressure vessel (RPV) steels from the ball indentation and tensile test data using the indentation energy to fracture (IEF) model and the relationships describing the effect of stress state on fracture. In the IEF model the fracture toughness is expressed as a function of the ball indentation test parameters and critical mean contact pressure. From the relationships among the stress components the fracture stress is derived as a function of stress triaxiality and flow property. In this approach the fracture stress calculated for the stress triaxiality of indentation deformation is assumed as the critical mean contact pressure. Indentation and tensile tests were performed on six RPV steels at transition temperatures of −160–25°C. The values of critical mean contact pressure were in the range 2500–2800 MPa. The temperature dependence of the estimated fracture toughness, K_{JC}, agreed well with that obtained by the master curve method of ASTM E 1921 using three-point bend (TPB) specimens. In addition, the critical fracture stresses were obtained by considering the stress triaxiality for the crack tip. All test materials revealed the values of the critical fracture stress ranging from 2100 to 2500 MPa.

1. Introduction

Many theories and models have been developed to measure the mechanical properties of materials from ball indentation tests [1–8]. The current status is that many fundamental mechanical properties replacing the tensile test data can be measured using ball indentation test technology [4–6]. However, since ball indentation on the ductile metals does not induce cracking even at very low temperatures, the estimation of fracture toughness using the indentation test has been rarely attempted for ductile metals [5]. Recently, the indentation energy to fracture (IEF) model was proposed to estimate the fracture toughness of ferritic steels from the ball indentation test data by the same authors [7,8]. The IEF model is based on the assumption that the indentation deformation energy per unit contact area up to a critical mean contact pressure is equal to the plastic energy portion of the fracture energy per unit area. In the model an imaginary fracture should be imposed to the indentation deformation because most ductile metals do not reveal cracking during indentation. The criterion for the imaginary fracture is that fracture occurs when the maximum contact pressure reaches the fracture stress of the material [7]. In the practical application of the IEF model, how to evaluate the fracture criterion has been the key procedure for obtaining correct fracture toughness values [9]. This study is aimed at the development of a methodology to evaluate the critical mean contact pressure, as a fracture criterion, from tensile test data.

* Corresponding author. Present address: Metal and Ceramics Division, Oak Ridge National Laboratory, P.O. Box 2008, Bldg. 5500, MS-6376, Oak Ridge, TN 37831, USA. Tel.: +1-423 576 7738; fax: +1-423 574 0641.
E-mail address: byunts@ornl.gov (T.S. Byun).

0022-3115/00/$ - see front matter
PII: S0022-3115(99)00197-X

In Ref. [7] it was shown that similar fracture toughness values were obtained from the standard fracture mechanics test and the IEF model. This result was explained by the fact that the indentation deformation reveals a very similar degree of stress triaxiality to the deformation ahead of the crack tip. The effect of stress state on the fracture behaviors of SA508-3 reactor pressure vessel (RPV) steel in the transition region has been investigated using notched round tensile specimens of various notch root radii [10]. The test results showed that the fracture stress and fracture strain are strongly dependent on the stress state (stress triaxiality); the fracture stress increases with the stress triaxiality, while the fracture strain decreases with the stress triaxiality. In the present work the fracture strain is expressed as an exponential function of stress triaxiality based on the experimental results [9–11] and the fracture stress is modeled as a function of stress triaxiality and flow property based on the relationships among the stress components. Then, the value of the critical mean contact pressure is evaluated using the fracture stress versus triaxiality relationship from the tensile test results and the stress triaxiality values in the indentation deformation.

This paper also includes the application results for six RPV steels including one SA533-B-1 steel and five SA508-3 steels. The stress triaxiality was evaluated for the indentation deformation. With the evaluated stress triaxiality, the critical mean contact pressure, fracture toughness, and transition (or reference) temperature were estimated for those RPV steels from the ball indentation test and tensile test data. In addition, the fracture stress was evaluated for the crack tip and discussed with relation to the effects of stress triaxiality.

2. Modeling

2.1. The IEF model

The mechanical properties measured from a specimen might be influenced by the strain rate and test temperature as well as by the specimen geometry and loading pattern, determining the stress state within the specimen. At a given strain rate and test temperature similar stress states might result in similar values of fracture toughness. Thus the agreement between the fracture toughness values obtained by the IEF model and the conventional fracture toughness testing was explained by the analogy of stress states in the two deformations [7,9].

Theoretically, the stress triaxiality, the ratio of mean stress to equivalent stress, is close to 0.4 at the moment of contact between the ball and the sample surface [2]. However, a FEM calculation showed that the stress triaxiality in the RPV steels reached about 2 at very small strain and increases to about 3 as the indentation depth increased [7]. It saturates nearly at an indentation depth of about 10% of the ball radius, which corresponds to about 9% plastic strain. FEM simulations and theoretical calculations on the deformation around the crack tip showed that the values of stress triaxiality were also in the range 1.9–3.3 [12–15]. In the IEF model it is postulated that the indentation energy per unit contact area to a critical point is related to the fracture energy of the material. The indentation energy to fracture was defined by Byun et al. [7]:

$$W_{\mathrm{IEF}} = \frac{4}{\pi d_{\mathrm{f}}^2} \int_0^{h_{\mathrm{f}}} P \,\mathrm{d}h, \tag{1}$$

where P is the applied load, h the indentation depth, h_{f} the critical indentation depth, and d_{f} is the critical chordal diameter of the indentation impression. This equation is easily integrated using a linear indentation load–depth (P–h) curve: $P = Sh$, where S is the slope of the curve. Using the definition of critical mean contact pressure and the Meyer law [3]:

$$p_{\mathrm{m}}^{\mathrm{f}} = \frac{4P_{\mathrm{f}}}{\pi d_{\mathrm{f}}^2}, \tag{2}$$

$$\frac{P_{\mathrm{f}}}{d_{\mathrm{f}}^2} = A\left(\frac{d_{\mathrm{f}}}{D}\right)^{m-2}, \tag{3}$$

where A is the material yield parameter, m the Meyer index, and D is the ball diameter, the IEF is expressed as a function of indentation parameters:

$$W_{\mathrm{IEF}} = \frac{2A^2D^2}{\pi S}\left(\frac{\pi p_{\mathrm{m}}^{\mathrm{f}}}{4A}\right)^{(2m-2)/(m-2)}. \tag{4}$$

W_{IFE} takes into account only the elastic–plastic deformation energy. However, the toughness parameters, such as Charpy impact energy and fracture toughness in the transition region, K_{JC}, have non-zero lower shelf values [16,17]. Thus in the transition regime the IEF model assumes that the fracture energy per unit area, W_{f}, is given by the two terms: the lower shelf, W_0, and the indentation energy to fracture [7]:

$$W_{\mathrm{f}} = W_0 + W_{\mathrm{IEF}}. \tag{5}$$

In addition, using the generalized Griffith theory under plane strain condition and the definition of fracture toughness for a crack in an infinite plate [18], the relationship between fracture energy and fracture toughness becomes

$$W_{\mathrm{f}} = \frac{K_{\mathrm{JC}}^2}{2E/(1-\nu^2)}, \tag{6}$$

where E is Young's modulus ($E = 207\,000–57T$ MPa, where T is the test temperature in °C) and ν is Poisson's ratio. Therefore, the fracture toughness, K_{JC}, is given by

$$K_{JC} = \left[\frac{2E}{1-\nu^2} \left\{ W_0 + \frac{2A^2D^2}{\pi S} \left(\frac{\pi p_m^f}{4A} \right)^{(2m-2)/(m-2)} \right\} \right]^{1/2}. \tag{7}$$

In this equation the values of A and S are known from indentation tests and the value of m can be obtained from the plastic flow curve; m is approximately equal to $n+2$, where n is the work-hardening exponent of a Hollomon-type flow curve [3]. Also, since the lower shelf of fracture toughness is 30 MPa$\sqrt{\text{m}}$ [16], Eq. (7) gives a value of 1975 J/m^2 as the lower shelf energy, W_0, with $E=210$ GPa, $\nu=0.28$, and $W_{IEF}=0$. The following sections suggest a methodology for calculating the value of p_m^f from tensile test results.

2.2. Fracture stress as a function of stress triaxiality

In the cracked or notched specimens a local constraint force would characterize the stress and strain fields around the crack tip (or notch root). The effects of a constraint or stress state on fracture have been emphasized by many authors [10–15,19–22] because it has been known that the fracture toughness decreases with increasing degree of constraint. The degree of constraint, or stress concentration, is often measured by the ratio of maximum principal stress to equivalent stress (denoted as C) [15,20] or more frequently by the stress triaxiality t [10–14,19–22]. In the present model it is intended to find a consistent relationship between the fracture behavior and the stress triaxiality and to apply it to different deformations. A symmetrical geometry of a round tensile specimen is used for simplicity in testing and for simple relations between stress components. The stress triaxiality is usually defined as the ratio of mean stress, σ_m, to the equivalent stress, σ_{eq}, [11,21]:

$$t = \frac{\sigma_m}{\sigma_{eq}}, \tag{8}$$

where the equivalent stress and mean stress are defined, respectively, as

$$\sigma_{eq} = \frac{1}{\sqrt{2}} \left[(\sigma_{11}-\sigma_{22})^2 + (\sigma_{22}-\sigma_{33})^2 + (\sigma_{33}-\sigma_{11})^2 \right]^{1/2}, \tag{9}$$

$$\sigma_m = \frac{\sigma_{11}+\sigma_{22}+\sigma_{33}}{3}. \tag{10}$$

Here, σ_{11}, σ_{22}, and σ_{33} are the principal stress components in the radial, circumferential, and axial directions, respectively. From the force equilibrium equations Bridgman and Miannay [23,24] derived the stress distributions in the axisymmetric notched specimens under a tensile force. This analysis hypothesizes that the strain distribution is approximately uniform across the minimum neck section. This hypothesis was drawn from the experimental observations and was also adopted in this model. Additionally, when plastic deformation is dominant, the strain components obey the incompressibility rule; $\varepsilon_{11}+\varepsilon_{22}+\varepsilon_{33}=0$. Therefore, with a load applied in the axial direction (33-direction), the relation between strain components is

$$\varepsilon_{33} = -2\varepsilon_{11} = -2\varepsilon_{22}. \tag{11}$$

With this relation, the equivalent strain becomes

$$\varepsilon_{eq} = \frac{\sqrt{2}}{3} \left[(\varepsilon_{11}-\varepsilon_{22})^2 + (\varepsilon_{22}-\varepsilon_{33})^2 + (\varepsilon_{33}-\varepsilon_{11})^2 \right]^{1/2} = \varepsilon_{33}. \tag{12}$$

For the above strain state, the relation between the two transverse stress components can be derived from the constitutive equations based on the total strain components as [10]

$$\sigma_{11} = \sigma_{22}. \tag{13}$$

Then, the equivalent stress and mean stress are given by

$$\sigma_{eq} = \sigma_{33} - \sigma_{11} = \sigma_{33} - \sigma_{22}, \tag{14}$$

$$\sigma_m = \sigma_{33} - \frac{2}{3}\sigma_{eq}. \tag{15}$$

The mechanical parameters that can be measured from a round bar specimen are the equivalent stress at fracture, σ_{eq}^f, the fracture stress in the axial direction, σ_f, and the fracture strain, ε_f. Using these parameters and Eqs. (8) and (15), the stress triaxiality at fracture can be expressed as follows:

$$t_f = \frac{\sigma_f}{\sigma_{eq}^f} - \frac{2}{3}. \tag{16}$$

Here, the value of the equivalent stress at fracture can be calculated from the flow curve of the material; $\sigma_{eq}^f = K(\varepsilon_f)^n$, where K and n are the strength coefficient and work-hardening exponent of the Hollomon-type flow curve.

For a failed round bar specimen, the fracture strain, ε_f, and fracture stress, σ_f, are calculated by the following relationships, respectively:

$$\varepsilon_f = 2\ln\left(\frac{d_0}{d_f}\right), \tag{17}$$

$$\sigma_f = \frac{4P_f}{\pi d_f^2}, \tag{18}$$

where d_0 and d_f are the initial diameter and the minimum diameter at fracture, respectively, and P_f is the fracture load. The fracture strain is known to decrease with increasing stress triaxiality. Many experimental results [9–11,21] implied that the variation of fracture

strain with stress triaxiality was described by an exponential function:

$$\varepsilon_f(t_f) = \alpha e^{-\lambda t_f}, \tag{19}$$

where λ is a material constant determining the stress triaxiality-dependence of fracture strain. According to a theoretical model [11], the value of λ is close to 3/2 for ductile fracture. However, the present model uses an empirical value obtained from the notched tensile bar specimens. α is a temperature-dependent parameter and therefore should be determined for each temperature using Eq. (19). In the present study the value of α is calculated from the test results of smooth tensile specimens, ε_f and t_f.

Eq. (16) indicates that the fracture stress is also a function of stress triaxiality. Since the fracture stress is defined as the maximum principal stress at fracture, it increases with constraint force (or stress triaxiality). Using Eqs. (16) and (19) and the Hollomon flow curve, the fracture stress is given as a function of stress triaxiality:

$$\sigma_f(t_f) = \left(t_f + \frac{2}{3}\right)\sigma_{eq}^f = \left(t_f + \frac{2}{3}\right)K\alpha^n e^{-\lambda n t_f}. \tag{20}$$

Note that all constants and variables in this equation can be obtained from tensile tests. Therefore, when the stress state of the deformation can be evaluated by a method, we can evaluate the fracture stress from a tensile test only.

2.3. Critical mean contact pressure in the ball indentation deformation

In the present model the critical mean contact pressure is adopted as a fracture criterion for the indentation deformation of ductile metals. The most important reason for this is that the parameter can easily be evaluated from empirically measurable values and well-known models without knowledge of detailed deformation fields under the indenter. From Eqs. (2) and (3) the critical mean contact pressure can be derived as follows:

$$p_m^f = \frac{4A}{\pi}\left(\frac{d_f}{D}\right)^n. \tag{21}$$

According to the relation between the equivalent strain, or the representative strain for the indentation deformation zone, and the ratio d/D [3], the fracture strain is given by

$$\varepsilon_f = 0.2\frac{d_f}{D}. \tag{22}$$

Since the relationships between stress components, Eqs. (13) and (14), can be applied to any axisymmetric loading conditions, the stress triaxiality for ball indentation deformation, t_f^{ID}, is defined by the same relationship as Eq. (16) with substituting the fracture stress in the axial direction, σ_f, with the critical mean contact pressure, p_m^f. Therefore, using the Hollomon equation and Eq. (22), the stress triaxiality for the indentation deformation is expressed by

$$t_f^{ID} = \frac{p_m^f}{\sigma_{eq}^f} - \frac{2}{3} = \frac{4A5^n}{\pi K} - \frac{2}{3}. \tag{23}$$

Then, from Eq. (20) the critical mean contact pressure becomes

$$p_m^f = \left(t_f^{ID} + \frac{2}{3}\right)K\alpha^n e^{-\lambda n t_f^{ID}}. \tag{24}$$

3. Experimental

The test materials comprise five SA508-3 RPV steels and one SA533-B-1 RPV steel. The chemical compositions of the steels are listed in Table 1 and the steels are in a quenched, tempered, and simulated post-weld heat-treated state. The JRQ and JFL are the reference materials of the International Atomic Energy Agency (IAEA) supplied for round robin testing [25], and the KFY3, KFY4, KFY5, and KFU4 are Korean RPV steels manufactured by Hanjung (Korea Heavy Industry and Construction).

The tensile tests for the smooth round bar specimens were conducted at temperatures of −160°C to room temperature (RT) to obtain the flow properties, which are needed for calculating the critical mean contact pressure and fracture toughness from ball indentation test data. The diameter of the gage section of the smooth

Table 1
Chemical compositions of RPV steels

Material	C	Mn	Si	Al	Ni	Cr	Mo	P	S	Cu	V	Re.
JRQ (SA533-B-1)	0.18	1.42	0.24	0.014	0.84	0.12	0.51	0.017	0.004	0.14	0.002	Rolled
JFL (SA508-3)	0.17	1.44	0.25	0.016	0.75	0.20	0.51	0.004	0.002	0.01	0.004	Forged
KFY3 (SA508-3)	0.17	1.39	0.08	0.004	0.77	0.04	0.49	0.007	0.003	0.05	0.005	Forged
KFY4 (SA508-3)	0.20	1.42	0.07	0.005	0.79	0.15	0.57	0.007	0.003	0.06	0.005	Forged
KFY5 (SA508-3)	0.21	1.24	0.25	0.008	0.88	0.21	0.47	0.007	0.002	0.03	0.004	Forged
KFU4 (SA508-3)	0.19	1.35	0.08	0.009	0.82	0.17	0.51	0.006	0.002	0.03	0.002	Forged

tensile specimen was 5 mm and the gage length was 30 mm. For the KFU4 steel, the tensile tests using the notched round bar specimens were also performed in the same temperature range to obtain the relationships between mechanical properties and stress triaxiality. In the notched specimens the diameter of the smooth section was 8 mm and the diameter of the notched section at a position of minimum cross-sectional area was 4 mm. The notch root radius varied from 0.25 to 3 mm for introducing various stress triaxiality values. This variation in the notch root radius resulted in the stress triaxiality range 0.6–2 at the point of initial deformation and 0.8–1.3 at fracture. The details about these tensile tests are described elsewhere [10].

For ABI tests, Charpy-sized rectangular bars (10 mm × 10 mm × 55 mm) were cut from the 1/4 thickness location of RPVs. Continuous indentation tests were performed in an automated ball indentation (ABI) test system of the Advanced Technology Corporation (model: PortaFlow-P1). In the ABI tests, the indenter used was a tungsten carbide (WC) ball having 0.508 mm diameter. The test temperatures were controlled in a double-walled bath by the injection of liquid nitrogen with an accuracy of ±2°C. The indentation tests were performed at temperatures of −160°C to RT (25°C) with an indentation speed of 0.01 mm/s (0.0004 inch/s).

4. Results and discussion

4.1. Tensile deformation and fracture

Table 2 contains the coefficients of flow curves, which are used for evaluating Eqs. (7), (20), and (24). Since the strength coefficient, K, is strongly dependent on temperature, the values for the RPV steels are given as linear functions of temperature, T (in °C). Meanwhile, the work-hardening exponent, n, is given as a constant for the test temperature range.

For the smooth tensile specimens, the values of fracture strain are calculated by Eq. (17) from the values of the initial and final diameters. Fig. 1 shows the temperature-dependence of fracture strain. All RPV steels reveal apparent ductile-to-brittle transitions at relatively low temperatures ranging from −160°C to −100°C. Although the amount of data is insufficient for a detailed conclusion, the transition temperature seems to be material-dependent. Above −100°C, however, the fracture strain shows a moderate dependence on temperature; actually, this temperature region can be regarded as an upper shelf region showing ductile fracture.

Table 2
Coefficients in the flow curves of RPV steels

Material	K (MPa)	n (average)	Temperature
JRQ	983–2.90T	0.162	−160°C < T < 0°C
JFL	971–2.72T	0.160	−160°C < T < 0°C
KFY3	897–2.62T	0.168	−160°C < T < 0°C
KFY4	893–2.49T	0.142	−160°C < T < 0°C
KFY5	1008–1.99T	0.156	−160°C < T < 0°C
KFU4	969–2.34T	0.153	−160°C < T < 0°C

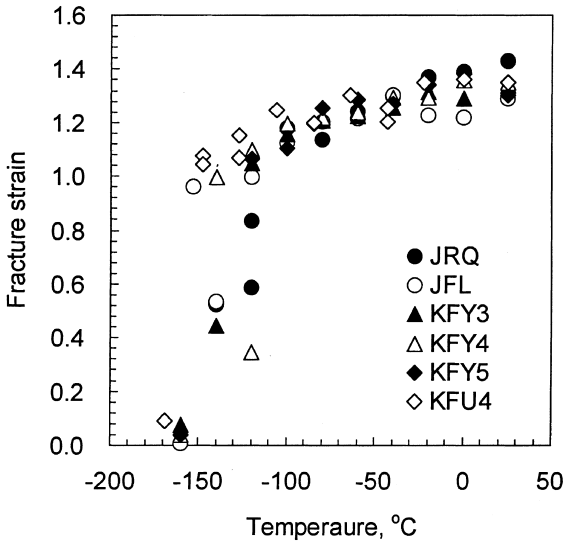

Fig. 1. Variation of fracture strain with temperature in the smooth tensile specimens.

Also, the values of fracture stress were calculated for the smooth specimens by Eq. (18) and the results are represented in Fig. 2. This figure indicates that the fracture stress is nearly independent of temperature as in other ferritic steels [26–28]. Fig. 2 also illustrates that most of the values of fracture stress are in the range of

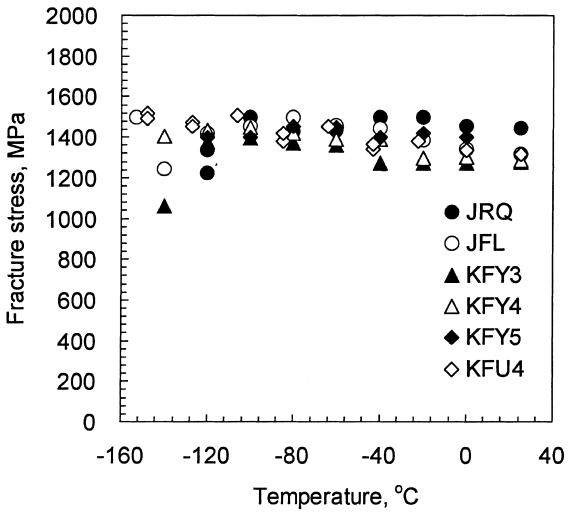

Fig. 2. Variation of fracture stress with temperature in the smooth tensile specimens.

1200–1500 MPa, even though they are obtained from the tests of six different RPV steels in the large temperature range from −160°C to 25°C. This result means that the values of fracture stress from smooth tensile specimens are much less than those evaluated at a crack tip, usually over 2000 MPa for similar steels [20,28,29]. This discrepancy between the fracture stresses in the different kinds of deformation may come from the effect of stress state. As will be discussed in detail later, the values of stress triaxiality at tensile fracture are in the range 0.33–0.72 and those at the crack tip are in the range 1.9–2.8. For the elastic plastic deformations in the RPV steels, the larger the stress triaxiality, the higher the fracture stress.

It is also noted that in the lower temperature region of around −150°C, the values of fracture stress reveal somewhat larger scatters. This temperature region is included in the transition temperature region of fracture strain as indicated in Fig. 1. It is a well-known fact that failure in the transition region is subjected to the cleavage fracture initiated in a probabilistic manner, and consequently the fracture parameters measured in the region reveal larger scatter [16,30,31].

4.2. Stress triaxiality in the tensile and ball indentation deformations

For uniaxial tensile testing, the value of stress triaxiality is evaluated to be 1/3 within uniform deformation range. After the initiation of necking, however, the neck constrains the deformation like a notch, and so the stress triaxiality at the necked section might increase to a higher value. Fig. 3 presents the values of stress triaxiality at fracture calculated using Eq. (16). In this plot, the stress triaxiality at fracture increases with increasing temperature, from 1/3 to 0.72. The minimum value of stress triaxiality, 1/3, appears frequently at temperatures lower than −100°C, which indicates the failure of the specimen before the initiation of necking. In the relatively high temperature region of −20°C to 25°C most of the values are in the range 0.6–0.7. In the notched bar specimens, a root radius of about 2–3 mm can induce this level of stress triaxiality [10].

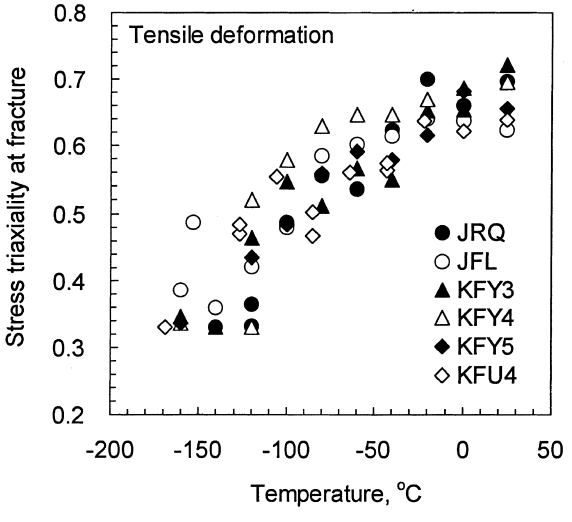

Fig. 3. Stress triaxiality at fracture in the tensile deformation.

From the ball indentation and tensile test results the values of stress triaxiality in the indentation deformation, averaged over the contact area, are calculated using Eq. (23) and presented in Fig. 4. When compared to the uniaxial tensile deformation, much higher stress triaxiality is evaluated for the indentation deformation. In the indentation deformation case, the stress triaxiality is insensitive to temperature, and thus the values averaged over a low temperature range from −160°C to −80°C are used for calculating the critical mean contact pressure. Table 3 contains the average values of stress triaxiality for the six test materials with the values of constraint ($C_f^{ID} = t_f^{ID} + 2/3$). Table 3 indicates that all

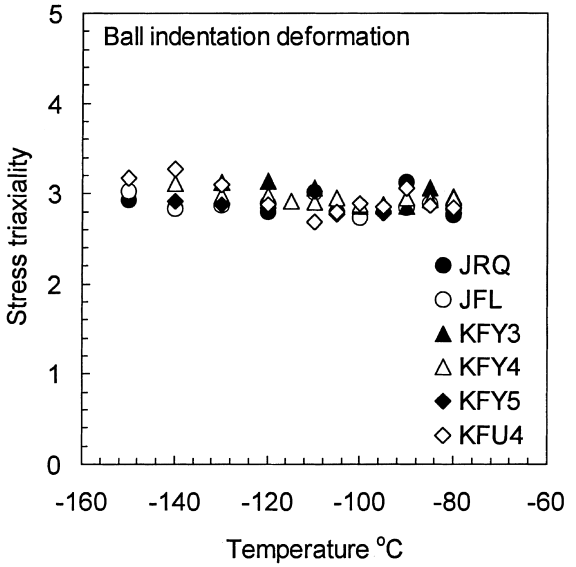

Fig. 4. Stress triaxiality in the ball indentation deformation.

Table 3
Stress triaxiality and critical mean contact pressure in the ball indentation deformation (average values in the temperature range of $\leqslant -80$°C)

Material	t_f^{ID}	C_f^{ID}	p_m^f (MPa)
JRQ	2.87	3.54	2671
JFL	2.88	3.55	2765
KFY3	3.00	3.66	2539
KFY4	2.95	3.62	2541
KFY5	2.86	3.53	2693
KFU4	2.94	3.61	2657

RPV steels reveal similar values, ranging from 2.86 to 3.0. It is also noted that these values are slightly higher than the values ahead of the crack tip; the finite element simulation for RPV steel showed that the stress triaxility at the crack tip was less than about 2.8 [7,13–15,19].

4.3. Fracture strain versus stress triaxiality relationship

The effect of stress triaxiality on fracture strain is illustrated in Fig. 5, in which the data are from KFU4 steel. Since the fracture stress of ferritic steel is nearly constant over the transition temperature region and the fracture toughness is dependent mainly on the fracture stress and fracture strain, the transition behavior of fracture toughness can be characterized by that of the fracture strain. Here, as seen in Fig. 5, the temperature-dependence of the fracture strain is described by the hyperbolic tangent curve [10]:

$$\varepsilon_f = A\left[1 + \tanh\left(\frac{T - T_{TR}}{B}\right)\right], \tag{25}$$

where $2A$ is the upper shelf value, T_{TR} is the transition temperature defined at $\varepsilon_f = A$, and $2B$ = transition temperature span. Table 4 contains the values of these parameters as well as the maximum stress triaxiality at fracture. Fig. 5 and Table 4 state that the fracture strain decreases and the transition temperature, T_{TR}, increases with increasing the stress triaxiality. There also exists a decreasing trend in the transition temperature span (or transition temperature region) as the stress triaxiality increases.

As stated earlier, to evaluate the critical mean contact pressure as a criterion for fracture, the relationship between the fracture strain and the stress triaxiality, Eq. (19), should be known for the test materials. The coefficients of the relationship were obtained from the experimental data of $2A$ (= upper shelf value of fracture strain), as seen in Fig. 6, in which the coefficient of the exponent, λ, is about 1.2. This value is similar to the theoretical value of 1.5 [11]. In the present calculation, the experimental value for λ, 1.2, is used for all temperatures and materials and, using Eq. (19), the value of α is calculated for respective temperatures and materials from the tensile test data. For the present RPV steels, α revealed values in the range 0.5–4 and increased with temperature.

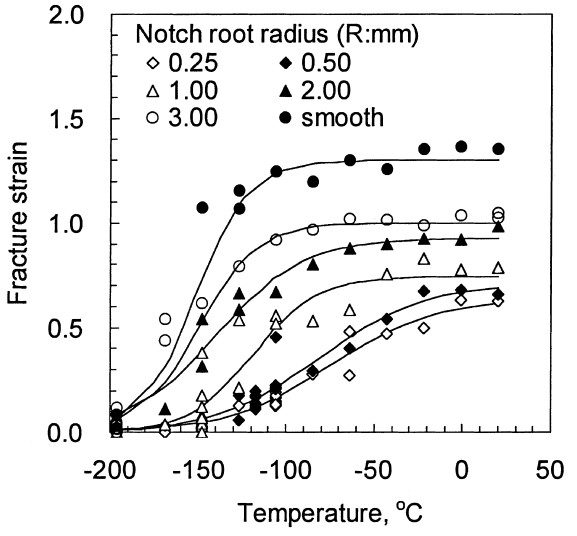

Fig. 5. Effect of stress triaxiaity on the transition behavior of fracture strain in the KFU4-SA508-3 forging steel.

Table 4
Fitting parameters of fracture strain versus temperature curves and stress triaxiality at fracture

R (mm)	t_f (at upper shelf)	$2A$ (= upper shelf value)	B	T_{TR} (°C)
0.25	1.26	0.628	59	−75
0.5	1.06	0.792	59	−81
0.75	1.10	0.756	40	−107
1.0	1.05	0.786	36	−119
1.5	0.97	0.939	50	−133
2.0	0.89	0.952	49	−140
3.0	0.87	1.025	33	−150
∞	0.65	1.283	30	−152

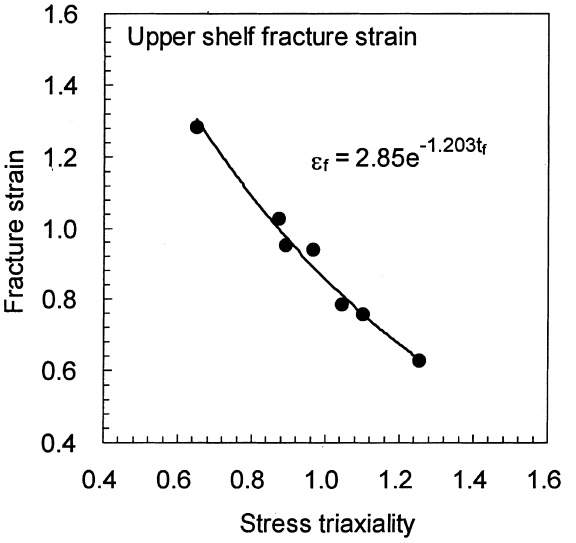

Fig. 6. Relationship between fracture strain and stress triaxiality.

4.4. Critical mean contact pressure

The values of critical mean contact pressure, p_m^f, were calculated by Eq. (24) and the results are illustrated in

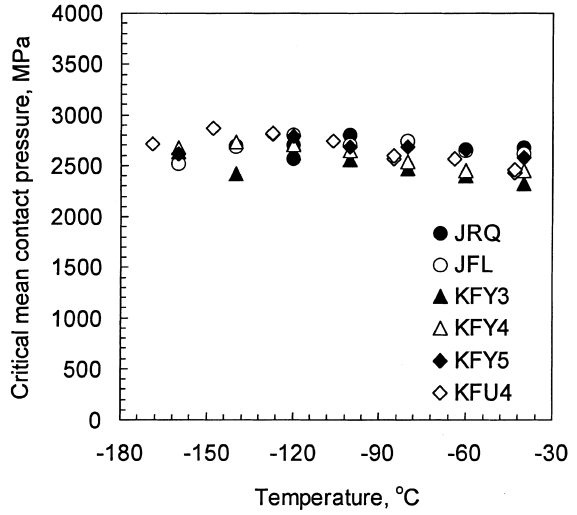

Fig. 7. Temperature dependence of critical mean contact pressure.

Fig. 7. This figure shows that the critical mean contact pressure is insensitive to the test temperature. Since the ratio between the local stress at the center of the impression and the mean contact pressure can be given as a constant of about 1.1 [7], the local fracture stress estimated at the center of the impression will be also temperature-insensitive. This result agrees with the fact that the critical fracture stress is nearly temperature-independent in the ferritic steels, and thus it is regarded as a material constant in many critical stress models on cleavage fracture [28,29].

On the other hand, since the transition temperature range changes with the stress triaxiality, as illustrated in Fig. 5 and Table 4, the transition temperature measured from the deformation and fracture at the crack tip or from the indentation deformation will be higher than that measured from uniaxial tensile testing. Fig. 1 states that the temperature range of -160°C to -80°C is evidently a transition region for both the tensile deformation and the ball indentation deformation. For these reasons, the values of critical mean contact pressure are averaged over the temperature range of -160°C to -80°C and the average value is regarded as a material constant; i.e., a fracture criterion of the material in the indentation deformation. Table 3 contains the average critical mean contact pressure estimated for the six RPV steels, ranging from 2500 to 2800 MPa.

4.5. Fracture toughness transition curves

The fracture toughness, K_{JC} in Eq. (7), was estimated from the results of ball indentation and tensile tests at various temperatures and the calculated values of critical mean contact pressure. According to the ASTM master curve method [16,32], the transition behavior of fracture toughness can be described by one parameter curve. For ferritic steels, the median curve is given by

$$K_{JC} = 30 + 70e^{0.019(T-T_0)}\ \text{MPa}\sqrt{\text{m}}, \tag{26}$$

where T_0 is the reference temperature and is regarded as a key material constant in determining fracture toughness in the transition region. Here, the transition curve of a generalized form is obtained by regression of the estimated K_{JC} data over a range of -160°C to -10°C:

$$K_{JC} = K_0 + Pe^{QT}\ \text{MPa}\sqrt{\text{m}}. \tag{27}$$

From this relationship the reference temperature is calculated to be

$$T_0 = \frac{Ln(P/70)}{Q}. \tag{28}$$

With a fixed value of K_0 ($=30$ MPa$\sqrt{\text{m}}$) the values of P, Q, and T_0 are calculated for each steel and are listed in Table 5. As shown in the previous work [7], most of the Q values are very similar to the coefficient in Eq. (16), 0.019, which is suggested by ASTM.

The parameter Q determines the shape of the fracture toughness transition curve, and the reference temperature, T_0, determines the position of the curve in the temperature axis. Since the calculated values of Q are similar for the six RPV steels, the estimated K_{JC} data of the steels will be located around the ASTM master curve if the fracture toughness is plotted as a function of the temperature relative to T_0: $T - T_0$. Fig. 8 illustrates this prediction; most estimated K_{JC} data are located between the 5% and 95% confidence curves.

Furthermore, the reference temperatures were evaluated for the same materials by the methodology of ASTM E 1921 using the Charpy-size three-point bend (TPB) specimens [16,25]. In Fig. 9, the estimated T_0 is compared with the data by TPB specimens. The difference between the two methods is less than 10°C. This result means that the present method can predict the reference temperature, a key parameter in the characteristics of fracture, with sufficient accuracy.

Table 5
Estimated fracture toughness transition curves of RPV steels

Material	K_0 (MPa$\sqrt{\text{m}}$)	P (MPa$\sqrt{\text{m}}$)	Q (°C^{-1})	T_0 (°C)
JRQ	30	236.9	0.0197	−61.9
JFL	30	360.7	0.0184	−90.1
KFY3	30	239.6	0.0194	−63.4
KFY4	30	410.8	0.0288	−61.4
KFY5	30	325.7	0.0191	−80.5
KFU4	30	318.5	0.0207	−73.1

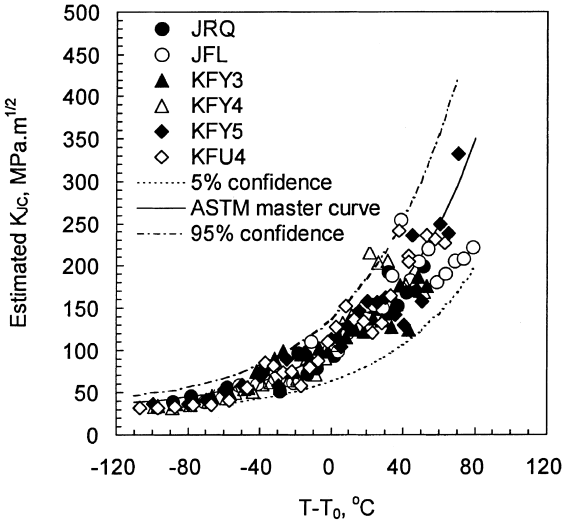

Fig. 8. Estimated K_{JC} versus $(T-T_0)$ data.

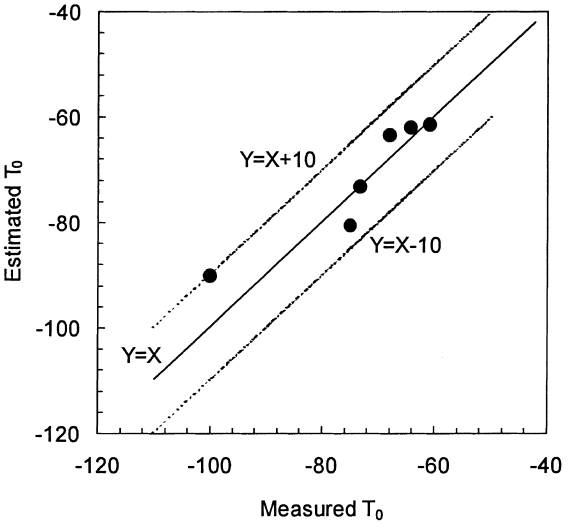

Fig. 9. Comparison of measured and estimated reference temperatures.

4.6. Fracture stress at crack tip

In Section 2.2 we derived the fracture stress for the axisymmetrical geometry as a function of stress triaxiality. Similarly, the fracture stress can be derived for the cracks in the standard fracture specimens, such as the compact tension (CT) and TPB specimens. Under the plane strain condition, Eq. (20) is changed to

$$\sigma_f(t_f) = \left(t_f + \frac{1}{\sqrt{3}}\right) K \alpha^n e^{-\lambda n t_f}. \tag{29}$$

In micro-fracture mechanics modeling the knowledge of critical fracture stress, σ_f^c, is important for a low-temperature application. Therefore, it is attempted to evaluate the stress triaxiality ahead of the crack tip as an approximate function of fracture toughness; subsequently, the critical fracture stress is evaluated using Eq. (29). In the deformation around a crack tip, the stress triaxiality increases with the work-hardening of the material, and the maximum stress triaxiality is determined by the strain-hardening capability [4,5,7]. Thus the lower bound of stress triaxiality can be derived from the stress fields before the initiation of plastic deformation. An analytical solution about elastic fields gives [7,33]

$$t_{\min} = \frac{2(1+v)}{3(1-2v)}. \tag{30}$$

Since Poisson's ratio, v, is about 0.28 for steels, $t_{\min}$ is calculated to be 1.94. Also, finite element simulations showed that the maximum stress triaxiality at a peak stress point ahead of the crack tip was about 2.8 for RPV steels [13]. This value is obtained when the deformation ahead of the crack tip reaches a fully plastic regime and the value of J-integral is greater than the fracture toughness of the material. On the other hand, the lower shelf and upper shelf values of fracture toughness are regarded as the minimum and maximum values of fracture toughness corresponding to the minimum and maximum values of stress triaxiality, respectively. The lower shelf of fracture toughness is 30 MPa$\sqrt{}$m as in Eq. (26) and the upper shelf of the present RPV steels is roughly 300 MPa$\sqrt{}$m [10]. Then, we can combine two points: $(K_{JC}, t_f) = (30, 1.94)$ and $(300, 2.8)$. From these data the stress triaxiality ahead of the crack tip is obtained as a power-law function:

$$t_f = 1.13(K_{JC})^{0.16}. \tag{31}$$

With this equation and the values of estimated K_{JC}, the critical fracture stress is evaluated for respective RPV steels and the results are presented in Fig. 10. It is noted again that the critical fracture stress is nearly temperature-independent in the transition region. Also, the values of critical fracture stress are averaged over the temperature range of -160°C to -80°C and are listed in Table 6. All test materials revealed values of critical fracture stress ranging from 2100 to 2500 MPa. A similar range of critical fracture stress, 2100–2900 MPa, was evaluated for similar quenched and tempered steels [29]. Especially, by a micro-fracture model the critical fracture stress of SA533-B-1 steel was predicted to be 2250 MPa [34]. The present method predicted a similar value of 2375 MPa for the SA533-B-1 steel (JRQ).

Table 6 also illustrates that the critical mean contact pressure is 1.12–1.16 times higher than the critical fracture stress. As assumed for the derivation of Eq. (31), the

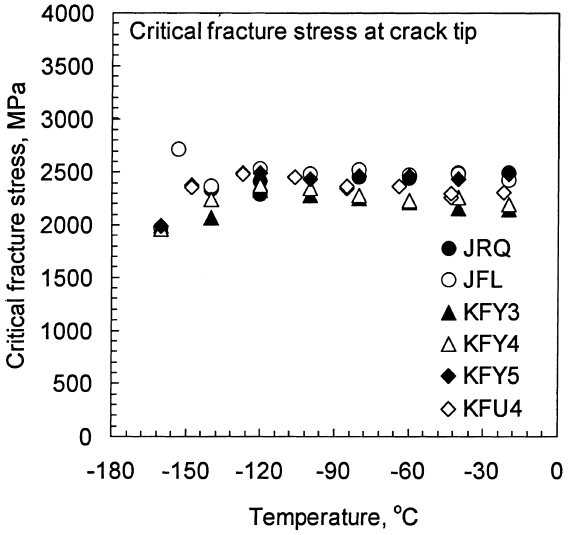

Fig. 10. Temperature dependence of the critical fracture stress at crack tip.

Table 6
Critical fracture stress at crack tip and the ratio to critical mean contact pressure (average values in the temperature range of $\leqslant -80°C$)

Material	σ_f^c (MPa)	p_m^f/σ_f^c
JRQ	2375	1.12
JFL	2432	1.14
KFY3	2185	1.16
KFY4	2268	1.12
KFY5	2369	1.14
KFU4	2375	1.12

stress triaxiality for a crack tip is in the range 1.94–2.8. The stress triaxiality in the indentation deformation ranges from 2.7 to 3.2 at the moment of the imaginary fracture. A simple analysis using Eq. (20) can show that the fracture stress increases by increasing the stress triaxiality in the work-hardening exponent range 0.14–0.17 (see Table 2). Furthermore, the constant in Eq. (20), 2/3, is higher than that in Eq. (29), $1/\sqrt{3}$. For these reasons, the critical mean contact pressure, p_m^f, is calculated to be higher than the critical fracture stress, σ_f^c.

5. Summary and conclusions

This paper proposed a methodology for estimating the fracture toughness of ferritic RPV steels in the transition region based on the IEF model and the relationships between the stress state and the fracture parameters. In this model, the fracture stress was expressed as a function of stress triaxiality and flow property; also, the fracture strain was given as an exponentional function of stress triaxiality, in which the constants were determined from smooth and notched tensile tests. The proposed method was applied to six RPV steels; the stress triaxialities at tensile fracture and indentation deformation, critical mean contact pressure, and critical fracture stress were evaluated using the function. The K_{JC}–T curves in the transition regime were also obtained for the six RPV steels and compared with the results from the standard testing with TPB specimens. From the application, some valuable results were obtained, as follows:

1. In the uniaxial tensile deformation, the fracture strain of the RPV steels revealed apparent ductile-to-brittle transition at relatively low temperatures, while the fracture stress was nearly independent of test temperature.
2. The stress triaxiality at the fracture of a smooth tensile bar was in the range of 1/3 to 0.72 depending on its ductility (or temperature). However, much higher stress triaxiality, in the range 2.86–3.0, was calculated for the indentation deformation.
3. The fracture strain obtained from the notched tensile specimens revealed that the fracture strain decreases and the transition temperature increases as the stress triaxiality increases.
4. The critical mean contact pressure of the RPV steels was also nearly independent of test temperature. For tested materials, the values at $-160°C$ to $-80°C$ were averaged and the average values were used for evaluating the fracture toughness using the IEF model. They were in the range 2500–2800 MPa.
5. In the plot of K_{JC} versus $T-T_0$, most estimated K_{JC} data were located between the 5% and 95% confidence lines. Also, the estimated values of T_0 were compared with those from the TPB specimens; the difference between the measured and estimated T_0 values was less than 10°C. These results suggest that the present method can be used for practical applications when the amount of the sample for standard fracture testing is restricted.
6. Finally, the fracture stresses estimated for the crack tip were in the range 2100–2500 MPa for the test materials.

Acknowledgements

This work has been carried out as a part of the Reactor Pressure Boundary Materials Project that is financially supported by the Korean Ministry of Science and Technology.

References

[1] R.A. George, S. Dinda, A.S. Kasper, Met. Progr. (1976) 30.
[2] H.A. Francis, J. Eng. Mater. Technol. 98 (3) (1976) 272.

[3] D. Tabor, J. Inst. Met. 79 (1951) 1.
[4] F.M. Haggag, R.K. Nanstad, D.N. Braski, in: D.L. Mariott, T.R. Mager, W.H. Bamford (Eds.), Innovative Approaches to Irradiation Damage and Fracture Analysis, ASME PVP-170, 1989, p. 101.
[5] F.M. Haggag, in: W.R. Corwin, F.M. Haggag, W.L. Server (Eds.), Small Specimen Test Techniques Applied to Nuclear Reactor Vessel Thermal Annealing and Plant Life Extension, ASTM STP 1204, 1993, p. 27.
[6] T.S. Byun, J.H. Hong, F.M. Haggag, K. Farrell, E.H. Lee, Int. J. Press. Vessel Piping 74 (3) (1998) 231.
[7] T.S. Byun, J.W. Kim, J.H. Hong, J. Nucl. Mater. 252 (1998) 187.
[8] F.M. Haggag, T.S. Byun, J.H. Hong, P.Q. Miraglia, K.L. Murty, Scr. Mater. 28 (4) (1998) 645.
[9] T.S. Byun, B.S. Lee, J.H. Yoon, J.H. Kim, J.H. Hong, in: Proceedings of the Fifth Workshop on Integrity of Reactor Components, Taejon, South Korea, 12–13 May, 1998, p. 391.
[10] S.H. Kim, T.S. Byun, B.S. Lee, J.H. Hong, I.S. Kim, in: Proceedings of the 12th Conference on Mechanical Behaviors of Materials, Chang-won, South Korea, 9–10 May, 1998, p. 203.
[11] M.S. Mirza, D.C. Barton, P. Church, J. Mater. Sci. 31 (1996) 453.
[12] H. Ma, Int. J. Fract. 89 (1998) 143.
[13] H. Kordisch, E. Sommer, W. Schmitt, Nucl. Eng. Design 112 (1989) 27.
[14] G. Wanlin, Eng. Fract. Mech. 51 (1) (1995) 51.
[15] G.Z. Wang, J.H. Chen, Metall. Trans. A 27 (1996) 1909.
[16] ASTM E1921-98: Test Method for the Determination of Reference Temperature, T_0, For Ferritic Steels in the Transition Range, 1998.
[17] R.O. Ritchie, W.L. Server, R.A. Wullaert, Metall. Trans. A 10 (1979) 1557.
[18] T.L. Anderson, Fracture Mechanics, CRC, Boca Raton, FL, 1995, p. 41.
[19] K.C. Koppenhoefer, R.H. Dodds Jr., Nucl. Eng. Design 162 (1996) 145.
[20] J.H. Chen, H. Ma, G.Z. Wang, Metall. Trans. A 21 (1990) 313.
[21] A.C. Mackenzie, J.W. Hancock, D.K. Brown, Eng. Fract. Mech. 9 (1977) 167.
[22] M. Zheng, X. Zheng, Theoretical Appl. Fract. Mech. 18 (1993) 157.
[23] P.W. Bridgman, Studies in Large Plastic Flow and Fracture, McGraw-Hill, New York, 1952.
[24] D.P. Miannay, Fracture Mechanics, Springer, New York, 1997, p. 114.
[25] J.H. Hong, B.S. Lee, J.H. Kim, T.S. Byun, B.W. Lee, Progress Report for the IAEA-CRP-IV on Assuring Structural Integrity of Reactor Pressure Vessels, Korean Contribution, Agency Research Agreement No. 9134, 1998.
[26] R. Sandstrom, Y. Bergstrom, Met. Sci. 18 (1984) 177.
[27] J.H. Chen, G.Z. Wang, C. Yan, H. Ma, L. Zhu, Int. J. Fract. 83 (1997) 139.
[28] J. Markin, A.S. Tetelman, Eng. Fract. Mech. 3 (1971) 151.
[29] Z. Xiulin, Eng. Fract. Mech. 33 (1989) 685.
[30] K. Wallin, T. Saario, K. Torronen, Met. Sci. 18 (1984) 13.
[31] W.S. Lei, W. Dahl, Int. J. Press. Vessel Piping 74 (1997) 259.
[32] S.S. Kang, S.H. Chi, J.H. Hong, J. Korean Nucl. Soc. 30 (4) (1998) 364.
[33] K. Hellan, Introduction to Fracture Mechanics, McGraw-Hill, New York, 1984, p. 7.
[34] J.F. Knott, Micro-mechanisms of Plasticity and Fracture, University of Waterloo, 1983, p. 261.